Journal of The Electrochemical Society

Operating EC-based Electrolytes with Li- and Mn-Rich NCMs: The Role of O_2-Release on the Choice of the Cyclic Carbonate

Journal of The Electrochemical Society, 2020 **167** 110505

Operating EC-based Electrolytes with Li- and Mn-Rich NCMs: The Role of O_2-Release on the Choice of the Cyclic Carbonate

Tobias Teufl,[1,z] Daniel Pritzl,[1] Patrick Krieg,[2] Benjamin Strehle,[1,*] Manuel A. Mendez,[2] and Hubert A. Gasteiger[1,]**

[1]*Chair of Technical Electrochemistry, Department of Chemistry and Catalysis Research Center, Technical University of Munich, D-85748 Garching, Germany*
[2]*BASF SE Ludwigshafen, New Battery Materials and Systems, D-67056 Ludwigshafen, Germany*

Li- and Mn-rich layered oxides are a promising class of cathode active materials (CAMs) for future lithium-ion batteries. However, they suffer from fast capacity fading in standard EC-containing electrolytes, and therefore fluorinated alternatives, such as FEC, are required to improve their full-cell performance, which unfortunately increases the cost of the electrolyte. In this study, we will analyze the reasons for the poor cycling performance of EC-containing electrolytes with CAMs that release lattice oxygen at high degrees of delithiation, i.e., either of Li- and Mn-rich NCMs (LMRNCMs) during activation or of NCMs at high cutoff voltages. By on-line electrochemical mass spectrometry (OEMS), we will show that the stability of EC towards *electrochemical* oxidation is sufficient up to potentials of ≈4.7 V vs Li^+/Li, but that its *chemical* reaction with lattice oxygen released from CAMs negatively affects cycle-life. Furthermore, we will show that the use of EC-based electrolytes above the onset potential for oxygen release leads to a resistance build-up causing a rapid "rollover" fading, while FEC does not show such a dramatic impedance increase. Last, we will demonstrate that the lattice oxygen release from NCM-622 above ≈4.5 V vs Li^+/Li requires the use of EC-free electrolytes for stable cycling.

 [DOI: 10.1149/1945-7111/ab9e7f]

Manuscript submitted April 6, 2020; revised manuscript received May 31, 2020. Published July 1, 2020. *This was paper 63 presented at the Seattle, Washington Meeting of the Society, May 13–17, 2018.*

Battery electric vehicles (BEVs) are a very promising approach to make future mobility sustainable and environmentally more friendly.[1,2] Lithium-ion batteries are currently used for essentially all BEVs, as they can achieve high energy densities and as they have already been used in customer electronics for many years.[2,3] However, for mass market penetration of BEVs, today's lithium-ion batteries (LIBs) need to be improved in terms of energy density, while lowering cost at the same time.[4] Hereby, one of the main requirements is the optimization of the cathode active material (CAM), as it is largely responsible for the limited energy density of LIBs and as it has a significant cost contribution to the overall battery cell.[4] One of the most promising future CAMs are Li- and Mn-rich NCMs (x $Li_2MnO_3 \cdot (1-x)$ $LiNi_aCo_bMn_cO_2$, with a + b + c = 1; often referred to as LMRNCMs) that are based on the layered LCO structure.[5–7]

While these materials can achieve high reversible capacities of >250 mAh g^{-1}, their practical cycling performance shows several issues that have hindered their commercialization so far.[8,9] It has been shown that all layered oxides release lattice oxygen from the surface upon their delithiation above ≈80% state-of-charge (SOC; here defined with reference to the total amount of potentially interchangeable lithium), leading to a drastic degradation of the CAM and of the electrolyte, accompanied by a rapid capacity fading.[10–12] Since Li- and Mn-rich NCMs have to be activated by charging them to more than ≈90% delithiation in order to access their high reversible capacities, LMRNCMs are always operated above the onset potential for lattice oxygen release, which results in a surface restructuration during the initial cycles.[13,14] Furthermore, Li- and Mn-rich NCMs are generally operated with upper potential limits of ≈4.7 V vs Li^+/Li, and therefore require specially formulated electrolytes to minimize capacity fading and impedance build-up,[13,15] whereby especially ethylene carbonate (EC) containing electrolytes lead to poor cycle-life of graphite//LMRNCM full-cells.

The research group of Jeff Dahn showed that EC-containing electrolytes are disadvantageous for graphite//NCM-424 full cells when charged to cell potentials >4.4 V;[16–19] they showed that replacing EC by a variety of different SEI (solid electrolyte interphase) forming carbonates could significantly improve the high-voltage performance of layered oxides.[18–20] In particular, they showed that fluorinated electrolytes (e.g., FEC) can strongly improve the high voltage performance in full-cells with layered oxide based CAMs, and thus evaluated EC-free electrolytes for high-voltage applications,[16,17] a concept that had already been investigated by Gmitter at al.[21] One of the hypotheses that can be found in the literature is that FEC might be less prone to *electrochemical* oxidation compared to EC, thereby leading to the superior cycling performance of FEC-based and EC-free electrolytes at high positive cutoff voltages.[22–24] Other researchers suggested that FEC leads to the formation of a passivating surface layer on the cathode active materials at high potentials;[25] however, detailed surface analysis by other groups could not prove the existence of such a passivating surface layer and FEC-based electrolyte did also not lead to an improved cycling performance of graphite//LNMO cells, which have an upper cutoff cell voltage of 4.8 V.[24,26,27] The advantage of EC-free electrolytes in combination with layered oxide based CAMs operated at high upper cutoff potentials where lattice oxygen is released[10,11,28] may also be related to a lesser chemical reactivity of, e.g., FEC with the released lattice oxygen or that the reaction products have a less detrimental effect on long-term performance. In this respect, Wandt et al.[28] showed that at least part of the released lattice oxygen is singlet oxygen that, as shown by Freiberg et al.,[29] *chemically* oxidizes EC to VC and H_2O_2, which in turn gets electrochemically oxidized at these potentials to protic species. Alternatively, other authors suggested a *chemical* oxidation mechanism of EC via a surface reaction between EC and activated oxygen present at the surface of layered oxides at high potentials.[30–32]

In this study, we will analyze the stability of EC and FEC towards *electrochemical* oxidation at high potentials, and we will carefully investigate the role of lattice oxygen release onto the cycle-life of LRMNCM and NCM cathodes when cycled in full-cells with either EC- or FEC-based electrolytes. Using a coin-cell based full-

*Electrochemical Society Student Member.
**Electrochemical Society Fellow.
[z]E-mail: tobias.teufl@tum.de

cell configuration with an electrolyte/CAM weight ratio (m_{ely}:m_{CAM}) of ≈1.6:1 that is the practically lowest ratio that can be achieved with coin-cells and that is reasonably close to that in commercial cells (≈0.35:1),[33] we will show that LRMNCMs have a far superior cycle-life when EC is replaced by FEC. On-line electrochemical mass spectrometry (OEMS) will be used to examine the *electrochemical* stability of EC- and FEC- based model electrolytes, which turns out to be essentially identical up to 5.0 V vs Li^+/Li. By implementing an LMRNCM pre-activation step prior to extended charge/discharge cycling, we will seek to prove that the effect of lattice oxygen release is far more detrimental in EC-based electrolytes compared to FEC-based electrolytes, and that this is the main failure mechanism when Li- and Mn-rich NCMs are cycled in EC-containing electrolytes. Last, we show that the cycling stability of NCM-622 in graphite//NCM-622 full-cells is identical for EC- and FEC-based electrolytes as long as the upper cutoff cell voltages are low enough to not lead to lattice oxygen release (e.g., at 4.35 V), whereas far inferior cycling stability is obtained with EC-based electrolytes once the upper cutoff cell voltage is high enough to lead to lattice oxygen release (shown to occur at full-cell voltages exceeding ≈4.4 V).[34]

Experimental

Electrode preparation for full-cell coin-cell cycling experiments.—NCM-622 with the composition $Li_{1+\delta}Ni_{0.6}Co_{0.2}Mn_{0.2}O_2$ ($\delta \approx 0.005$–0.05) and a BET area of ≈0.4 $m^2\ g^{-1}$ as well as Li- and Mn-rich NCM (LMRNCM) with the composition 0.33 li_2MnO_3 · 0.67 $liMeO_2$ (Me = Co, Ni, Mn)[13] and a BET area of ≈4.5 $m^2\ g^{-1}$ were both obtained from BASF SE (Germany). While the exact composition cannot be shared, the $LiMeO_2$ had the exact same composition as used in the study by Strehle et al.[14]

For coin-cell testing of LMRNCM cathodes, inks for cathode electrode preparation consisted of 92.5 wt% CAM (BASF SE, Germany), 3.5 wt% polyvinylidene-fluoride binder (PVDF, Solef 5130, Solvay, Belgium), 2 wt% conductive carbon (Super-C65, Timcal, Switzerland; BET area of ≈62 $m^2\ g^{-1}$), and 2 wt% graphite (SFG6L, Timcal, Switzerland; BET area of ≈17 $m^2\ g^{-1}$). The materials were dispersed in N-methyl pyrrolidine (NMP, anhydrous, Sigma-Aldrich, USA) and coated onto aluminum foil (16 μm). Dried electrodes were calendered to a density of 2.3 g cm^{-3} and had a final electrode thickness of ≈20 μm. For charge/discharge cycling tests, electrodes with a diameter of 14 mm were punched out; they had an active material loading of ≈6.5 mg cm^{-2}, corresponding to ≈1.6 mAh cm^{-2} (based on a nominal reversible capacity of 250 mAh g^{-1}).

For coin-cell testing of NCM-622 cathodes, inks consisted of 94 wt% CAM (BASF SE, Germany), 3 wt% polyvinylidene-fluoride binder (PVDF, Solef 5130, Solvay, Belgium), and 3 wt% conductive carbon (Super-C65, Timcal, Switzerland; BET area of ≈62 $m^2\ g^{-1}$). The materials were dispersed in N-methyl pyrrolidine (NMP, anhydrous, Sigma-Aldrich, USA) and coated onto aluminum foil (16 μm). Dried electrodes were calendered to a density of 3.2 g cm^{-3} and had a final electrode thickness of ≈32 μm. For charge/discharge cycling tests, electrodes with a diameter of 14 mm were punched out; they had an active material loading of ≈10.1 mg cm^{-2}, corresponding to ≈1.6 mAh cm^{-2} (based on a nominal reversible capacity of 160 mAh g^{-1}).

Graphite electrodes used with Li- and Mn-rich NCM based cathodes were commercial electrodes with a graphite loading of ≈6.7 mg cm^{-2}, corresponding to ≈2.4 mAh cm^{-2} (based on a theoretical capacity of 360 mAh g^{-1}), while the commercial graphite electrodes used with the NCM-622 based cathodes had a higher graphite loading of ≈8.3 mg cm^{-2} (corresponding to ≈3.0 mAh cm^{-2}) to guarantee sufficient balancing up to the upper cutoff cell voltage of 4.6 V. Please note that the rather high N/P ratios of 1.5 for the Li- and Mn-rich NCM and 1.875 for NCM-622 was chosen in order to make sure that no additional effects, such as Li-plating, are introduced. For charge/discharge cycling tests, graphite electrodes with a diameter of 15 mm were punched out. All anode and cathode electrodes were dried overnight under vacuum in an oven within the glovebox (O_2, H_2O < 0.1 ppm, MBraun, Germany) at 120 °C and were not exposed to air after the drying procedure.

Cell assembly and charge/discharge cycling procedure.—Galvanostatic cycling was carried out in 2032-type coin-cells (Hohsen Corp., Japan) at 25 °C in a temperature-controlled oven (Binder, Germany) and using a battery cycler (Series 4000, Maccor, USA). For full-cell experiments in 2032 coin-cells, a graphite anode with a diameter of 15 mm and a cathode with a diameter of 14 mm were assembled (see above) with one polyethylene separator (2500, Celgard, USA) and with 14 μl (for Li- and Mn-rich NCM) or 21 μl (for NCM-622 due to the higher CAM loading) of electrolyte. The electrolytes used were prepared by BASF SE (Germany) and are either FEC:DEC (2:8 g:g) with 1 M $LiPF_6$ (at a density of ≈1.14 g cm^{-3}) or EC:DEC (2:8 g:g) with 1 M $LiPF_6$ (at a density of ≈1.13 g cm^{-3}); this equates to an electrolyte to CAM mass ratio of m_{ely}:m_{CAM} ≈ 1.6:1 for both the LMRNCM and the NCM-622 based coin-cells.

After assembly, all cells were left for a rest period of 2 h prior to charge/discharge cycling and C-rates are referenced to a nominal capacity of 250 mAh g^{-1} for cells with LRMNC cathodes and to 160 mAh g^{-1} for cells with the NCM-622 cathodes. The full-cells with LRMNCM cathodes were activated in the first cycle at a C-rate of C/15 to 4.7 V with a constant-current procedure (CC) and then discharged at C/15 to 2.0 V (CC); in subsequent cycles, the upper cutoff cell voltage was reduced to 4.6 V. Afterwards, 3 cycles with a 0.1 C CC charge and 0.1 C CC discharge were applied. This was followed by a rate test for which the cell was charged/discharged for 2 cycles each at 0.3 C (CCCV)/0.5 C (CC), 0.7 C (CCCV)/1 C (CC), 0.7 C (CCCV)/2 C (CC), 0.7 C (CCCV)/3 C (CC) and 0.7 C (CCCV)/1 C (CC) again, whereby all CV-steps were terminated after 1 h or when the current dropped below 0.01 C. After the rate test, a cycle-life test was conducted, starting with 3 cycles at 0.1 C CC charge and 0.1 C CC discharge, followed by 30 cycles at a charge rate of 0.7 C (CCCV) and a discharge rate of 1 C (CC), whereby the CV-step is defined as above. This sequence of 3 slow and 30 fast discharge cycles was repeated several times. For the NCM-622 full-cells, the same cycling procedure was used, but with identical upper cutoff cell voltages for all cycles, whereby two sets of cells were charged between either 3.00 V–4.35 V or 3.00 V–4.60 V, respectively.

Some of the LMRNCM cathode electrodes were pre-activated prior to cycling. For this, the first charge/discharge cycle (C/15 CC charge to 4.7 V and C/15 CC discharge to 2.0 V) was carried out in a single-layer pouch-cell with a graphite anode and with a capacity of ≈40 mAh and an area of ≈25 cm^2. The single-layer pouch-cells were assembled with the exact same materials, using one polyethylene separator (2500, Celgard, USA) and 1 ml of electrolyte, using either the FEC:DEC (2:8 g g^{-1}) plus 1 M $LiPF_6$ electrolyte or the EC:DEC (2:8 g g^{-1}) plus 1 M $LiPF_6$ electrolyte (BASF SE, Germany), i.e., the same electrolytes that are used for the above described coin-cell cycling test. While the activation in the pouch-cells was carried out under the same cycling conditions as in the coin-cells, the pouch-cells were degassed twice during the first cycle, namely at 4.0 V during charge and at 4.0 V during discharge. After this pre-activation cycle, the discharged cell was opened, and coin-cell electrodes were punched out (anode 15 mm diameter, cathode 14 mm diameter). The LMRNCM cathodes and the graphite anodes were afterwards washed in pure DEC (electrodes were placed in ≈10 ml DEC, mixed, and left to rest there for ca. 10 min; the washing routine was repeated a second time with fresh DEC), and coin-cells were assembled from the pre-activated electrodes. The pre-activated coin-cells were assembled with the same amount of electrolyte that was used for the above described coin-cell cycling test (i.e., 14 μl) and with the same type of freshly punched separator. Subsequently, these coin-cells were cycled with the same procedure

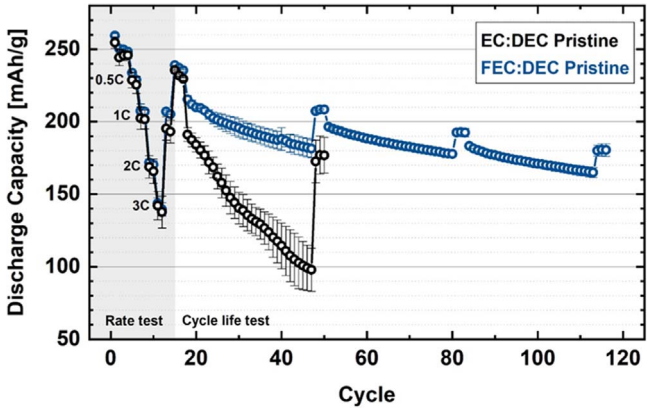

Figure 1. Charge/discharge cycling of graphite//LMRNCM coin-cells (≈2.4 mAh cm^{-2}//≈1.6 mAh cm^{-2}) at 25 °C, with 14 μl of either FEC:DEC (2:8 g:g) with 1 M $LiPF_6$ (blue symbols/lines) or EC:DEC (2:8 g:g) with 1 M $LiPF_6$ (black symbols/lines), corresponding to m_{ely}:m_{CAM} ≈ 1.6:1, and a Celgard 2500 separator. Activation was carried out at C/15 (CC) between 2.0–4.7 V, followed by a rate test (discharge rates are indicated in the figure) between 2.0–4.6 V. After these initial cycles (marked by the gray shaded area), a longer-term cycling sequence was carried out, starting with 3 cycles at 0.1 C (CC) charge and 0.1 C (CC) discharge followed by 30 cycles at 0.7 C (CCCV) charge and 1 C discharge (CC) between 2.0–4.6 V; this sequence was repeated several times, ending with 3 cycles at 0.1 C (CC) charge and 0.1 C (CC) discharge. The error bars represent the minimum/maximum between three independent repeat experiments.

as described above, except that the initial C/15 charge/discharge cycle (4.7–2.0 V) was omitted, as that had already been carried out during pre-activation in the pouch-cell.

On-line electrochemical mass spectrometry (OEMS) electrodes & setup.—For OEMS experiments, working electrodes were coated onto a stainless-steel mesh, as a porous current collector is required to allow for a fast diffusion of gases released from the working electrode to the capillary-leak inlet into the mass spectrometer of the OEMS.[14] NCM-622 working electrodes were prepared by dispersing 96 wt% NCM-622 (see above), 2 wt% conductive carbon (Super-C65, Timcal, Switzerland), and 2 wt% PVDF binder (Kynar HSV 900, Arkema, France) in NMP (anhydrous, Sigma-Aldrich, USA). A high solid content of 71% for the slurry was chosen to enable coating onto the porous stainless-steel mesh (SS316, aperture 26 μm, wire diameter 25 μm, The Mesh Company Ltd., UK). The slurry was coated with a wet film thickness of 20 μm onto the stainless-steel mesh, yielding an NCM-622 loading of ≈8.5 mg cm^{-2}. Electrodes for OEMS experiments were punched out with a diameter of 15 mm (resulting in a total of 15 mg NCM-622 per electrode) and compressed for 20 s with 2.5 tons.

The carbon black working electrodes for the OEMS measurements were prepared by dispersing 1.0 g conductive carbon (Super-C65, Timcal, Switzerland) and 1.0 g PVDF binder (Kynar HSV 900, Arkema, France) in 18 g NMP (anhydrous, Sigma-Aldrich, USA). The slurry was coated with a wet film thickness of 240 μm onto a polyethylene separator (Celgard 2500, USA), yielding a carbon loading of ≈0.8 mg_C cm^{-2}. Electrodes for OEMS experiments were punched out with a diameter of 15 mm. Based on the total amount of carbon black in the electrode (1.4 mg) and its BET area (62 m^2 g^{-1}), the total carbon surface area equates to 0.088 m^2, all anode and cathode electrodes were dried overnight under vacuum in an oven within the glovebox (O_2, H_2O < 0.1 ppm, MBraun, Germany) at 120 °C and were not exposed to air after the drying procedure.

For the OEMS measurements with a NCM-622 working electrode, a one-compartment OEMS cell design was used.[35] One-compartment OEMS cells were assembled with a lithium metal counter electrode (punched to 17 mm diameter), a glassfiber separator (200 μm thickness and punched to 20 mm diameter, VWR, Germany), an NCM 622 working electrode (see above), and 300 μl of electrolyte. The here used FEC-only or EC-only model electrolytes each contained 1.5 M $LiPF_6$ (BASF SE, Germany). The cells were connected to the mass spectrometer, held for 4 h at OCV (open circuit voltage), and then charged to 5.0 V vs Li^+/Li at a C/15 rate (C-rates here are calculated based on a nominal capacity of 160 mAh g^{-1}).

For the OEMS measurements on the oxidative stability of the EC-only and FEC-only electrolytes, carbon black based working electrodes (see above) were used in combination with a two-compartment OEMS cell, for which the working and the counter electrode compartments are separated by a lithium-ion conductive glass ceramic (Ohara Corp., Japan).[36] This cell setup allows to quantify the potential-dependent gas formation on the working electrode without interference from any gases that might be evolved at the counter electrode, and it also avoids any crosstalk effects; this is important to determine the exact onset of the electrochemical oxidation of the electrolyte on the carbon working electrode (for further details see Ref. 36). The two-compartment OEMS cells were assembled as follows. The counter electrode compartment was assembled with a lithium metal counter electrode (punched to17 mm diameter), a glassfiber separator (200 μm thickness and punched to 20 mm diameter, VWR, Germany), and 200 μl of electrolyte (LP57, BASF SE, Germany). After covering this counter electrode compartment with the sealed Ohara glass, the working electrode compartment was assembled with a polyester separator (punched to 20 mm diameter, Freudenberg, Germany), the carbon black working electrode (see above), and 100 μl of FEC-only or EC-only model electrolytes, each with 1.5 M $LiPF_6$ (BASF SE, Germany). The two-compartment cells were connected to the mass spectrometer, held for 4 h at OCV, and then charged to 5.5 V vs Li^+/Li at a scan rate of 0.1 mV s^{-1}.

For quantification of the mass spectrometer currents, a calibration gas containing H_2, O_2, CO_2, C_2H_4 (each 2000 ppm) in argon (Linde AG, Germany) was used. All currents were normalized to the current at m/z = 36 (Ar isotope) in order to correct for effects of minor pressure and temperature deviations; the currents for m/z = 32 (O_2) and for m/z = 44 (CO_2) normalized by the[36]Ar signal were then converted into gas concentration. Considering the internal volumes of the here used one-compartment (≈11 cm^3) and two-compartment cells (≈10 cm^3), the total moles of evolved gas were calculated from the measured concentrations using the ideal gas law, and then referenced to either the total BET surface area of the carbon black working electrodes or to the total NCM-622 mass of the NCM-622 working electrodes.

Results and Discussion

Full-cell performance of Li- and Mn-rich NCMs in EC- and FEC-based electrolytes.—To evaluate the actual cycling performance and the cycle-life of cathode active materials in combination with different electrolytes, it is crucial that the materials are tested under practically relevant conditions, i.e., in full-cells with a reasonable areal capacity, a proper anode/cathode balancing, and an electrolyte/CAM ratio that is as close as possible to large-format cells. For example, Wagner et al.[33] showed that the mass ratio of electrolyte to cathode active material in large-format commercial cells is on the order of m_{ely}:m_{CAM} ≈0.35:1. In a recent study by Günter et al.[37] with large-format graphite//NCM-111 cells, the best compromise between energy density and energy density retention over 500 cycles was at a pore volume filling factor of ≈1.2/1 (defined as ratio of electrolyte volume to the total pore volume of the electrodes and the separator), corresponding to m_{ely}:m_{CAM} ≈0.4:1; while higher m_{ely}:m_{CAM} ratios still showed a somewhat improved (i.e., lowered) impedance build-up over cycling, the resulting energy density was lower due to increased weight of the cell. These m_{ely}:m_{CAM} ratios are ≈20–30 times lower than what is typically used in coin-cell testing (m_{ely}:m_{CAM} ranging from ≈7:1 to ≈11:1 when using the typical ≈100 μl of electrolyte with 2032-type coin-cells). In order to most closely approach the value of large-format

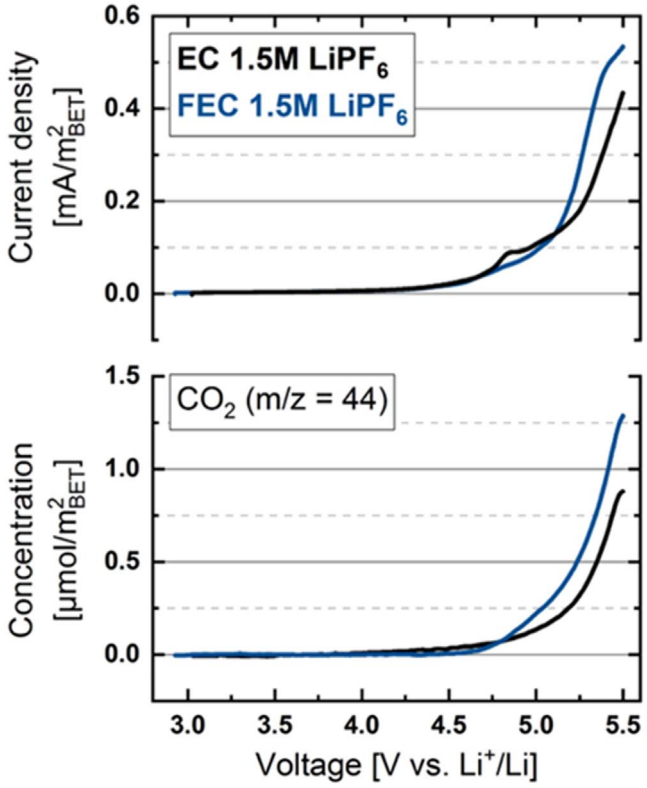

Figure 2. Anodic current (upper panel) and CO_2 evolution (lower panel) versus potential (referenced to Li^+/Li) recorded on a carbon black working electrode with either EC-only (pure EC + 1.5 M $LiPF_6$) or FEC-only (pure FEC + 1.5 M $LiPF_6$) electrolytes at 25 °C. A linear potential scan (0.1 mV s^{-1}) was carried out from OCV (≈3 V vs Li^+/Li) to 5.5 V vs Li^+/Li. The OEMS experiments were performed in a sealed two-compartment cell with a lithium counter electrode (see Experimental section); both the current and the amount of evolved CO2 are normalized to the total BET surface area of the carbon black electrode (0.088 m^2).

cells, we limited the amount of electrolyte in this study, using a ratio of m_{ely}:m_{CAM} ≈1.6:1, which is the lowest ratio with which we could still obtain reproducible coin-cell data and which is within a factor of ≈4–5 of large-format cells.

A Li- and Mn-rich NCM (LMRNCM) with the composition 0.33 li_2MnO_3 · 0.67 $liMeO_2$ (Me = Ni, Co, Mn) was used for full-cell cycling, whereby the composition of this CAM had been optimized with regards to minimizing its gassing during cell formation.[13] Figure 1 shows the capacity fading of this LMRNCM cycled with two different electrolytes, namely either EC:DEC (2:8 g:g) with 1 M $LiPF_6$ (black symbols/lines) or FEC:DEC (2:8 g:g) with 1 M $LiPF_6$ (blue symbols/lines). While the discharge capacity during the initial formation cycle (cycle 1) and the subsequent rate test (marked by the gray shaded area) is rather similar for the two electrolytes, it can be seen that during extended cycling at 0.7 C charge and 1 C discharge (starting from cycle #18), the cell with the EC-based electrolyte shows a rapid capacity fading which resembles the "rollover" failure mechanism that was discussed by Burns et al.[38] who ascribed it to a cell impedance build-up. In general, the term "rollover" failure describes the phenomenon that despite a still reasonable capacity retention at low C-rates, charge/discharge at high C-rates is not possible anymore due to high cell impedance. Interestingly, this is not observed with the FEC-based electrolyte. Specifically, the cells with the EC-based electrolyte (black symbols/lines, Fig. 1) show a rapid capacity decay during 1 C discharge cycling from 191 ± 5 mAh g^{-1} in cycle #18 to only 98 ± 15 mAh g^{-1} in cycle #47 (i.e., only 51% retention at 1 C over 30 cycles), while the cells with FEC-based electrolyte (blue symbols/lines) do not only show a higher capacity of 215 ± 3 mAh g^{-1} in cycle #18, but also a much better capacity retention with 165 ± 3 mAh g^{-1} after 113 cycles (i.e., 77% capacity retention at 1 C over 90 cycles at 1 C).

In order to differentiate between impedance related losses versus the loss of active lithium, three C/10 cycles were included in the long-term cycling procedure after every set of 30 cycles at 1 C discharge rate. The premise of this testing approach is the following: if the capacity fading is predominantly due to an impedance build-up (the origin of the "rollover" failure), the difference between the 0.1 C and the 1 C discharge capacity over the cycle-life test would be expected to increase; on the other hand, this difference should remain roughly constant if the capacity fading is predominantly due to a loss of active lithium. For the cells with the EC-based electrolyte (black symbols/lines, Fig. 1), the difference between the C/10 and the 1 C discharge capacity increases dramatically between the beginning of the longer-term cycling test (near cycle #20) and the end of testing (near cycle #50), which clearly indicates an impedance build-up in this electrolyte. Here it should be noted that cycling of these cells was stopped after this first cycle-life sequence, as the capacity retention had dropped below 50%. In contrast, the cells with the FEC-based electrolyte (blue symbols/lines) show an essentially constant difference between the 0.1 C and the 1 C discharge capacity over the course of cycling, indicative of a capacity fading mechanism that is largely due to the loss of active lithium. In summary, the analysis of Fig. 1 suggests that the comparatively strong capacity fading in cells with EC-based electrolyte is due to an impedance build-up and reflects the "rollover" fading reported for graphite//NCM cells cycled to high upper cutoff cell voltages.[10,38]

It has been shown in the literature that EC-based electrolytes do not provide long-term cycling stability when NCM materials are cycled in graphite//NCM cells to cell potentials exceeding 4.4 V[16] (corresponding to ≈4.5 V vs Li^+/Li), and many approaches have been made to design EC-free electrolytes with improved high voltage stability.[20,21] The underlying hypothesis is that the oxidative stability of EC at high voltages is inferior to that of FEC and other fluorinated solvents.[20,22–24,39] In this context, however, it is surprising that the cycling performance of full-cells with a high voltage spinel (LNMO, operated at 4.9 V vs Li^+/Li) cannot be improved by the addition of FEC to EC-based electrolyte[26] or by entirely replacing EC with FEC.[27] For this reason, we will next evaluate the oxidative stability of EC and FEC with 1.5 M $LiPF_6$ on a pure carbon electrode in order to get direct information on their oxidative stabilities.

Oxidative stability of EC and FEC on a carbon black working electrode.—In order to investigate the onset potential for the oxidation of EC and FEC, we investigated EC-only and FEC-only electrolytes with 1.5 M $LiPF_6$ (note that EC-only and FEC-only electrolytes were chosen because the quantification of the OEMS signals is more precise in the absence of the high-vapor pressure linear alkyl carbonates[40]). For this, we performed on-line electrochemical mass spectrometry (OEMS) using carbon black working electrodes without any cathode active material, monitoring both the current response and the CO_2 evolution from electrolyte oxidation (note that for electrolytes with $LiClO_4$ salt, ≈50% of the observed CO_2 is due to carbon rather than electrolyte oxidation,[40] but more recent studies showed that in the case of $LiPF_6$ salt, more than 95% of the evolved CO_2 derive from the oxidation of the electrolyte).[41] Following not only the current but also the CO_2 signal is necessary to differentiate between electrolyte oxidation and other possible parasitic reactions, such as PF_6^- intercalation into the carbon black. Furthermore, we use a sealed two-compartment cell setup that avoids crosstalk between the electrodes and allows to detect only the gases produced by the oxidation of the electrolyte on the carbon black working electrode, without interference from electrolyte reduction products that are formed at the lithium counter electrode (the setup is reported elsewhere[36]). Figure 2 shows the current profile (upper panel) and the CO_2 evolution (lower panel, based on m/z = 44) for FEC-only (FEC + 1.5 M $LiPF_6$) and for EC-only (EC + 1.5 M $LiPF_6$) electrolyte during a linear potential scan experiment

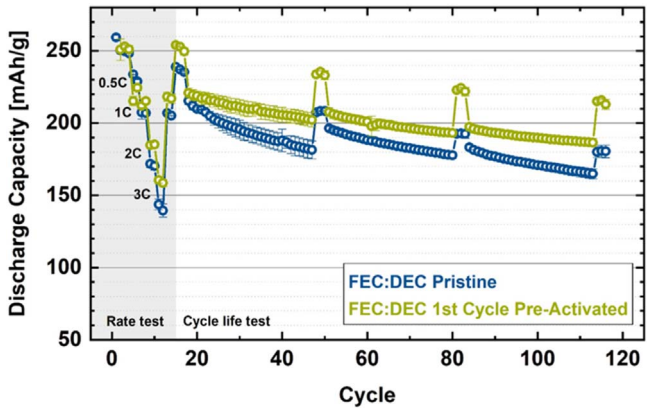

Figure 3. Charge/discharge cycling of pristine (blue symbols/lines) and pre-activated (green symbols/lines) graphite//LMRNCM coin-cells (≈2.4 mAh cm^{-2}//≈1.6 mAh cm^{-2}) at 25 °C, using 14 μl FEC:DEC (2:8 g:g) with 1 M $LiPF_6$ and a Celgard 2500 separator. For cells with pristine electrodes, the first-cycle activation was carried out at C/15 (CC) between 2.0–4.7 V (identical to the data shown in Fig. 1); for cells with pre-activated electrodes, the first-cycle pre-activation was conducted in a pouch-cell, then the electrodes were washed, punched to the size required for coin-cells, and finally reassembled in coin-cells with fresh electrolyte and a fresh separator (no further activation cycle was conducted in this case, so that there are no data for cycle #1 with pre-activated electrodes). Both types of cells then underwent the same cycling procedure as that used in Fig. 1: a rate test (discharge rates are indicated in the figure) between 2.0–4.6 V (marked by the gray shaded area), then a longer-term cycling sequence starting with 3 cycles at 0.1 C (CC) charge and 0.1 C (CC) discharge followed by 30 cycles at 0.7 C (CCCV) charge and 1 C discharge (CC) between 2.0–4.6 V (this sequence was repeated several times, ending with 3 cycles at 0.1 C (CC) charge and 0.1 C (CC) discharge). The error bars represent the minimum/maximum between three independent repeat experiments.

from OCV (≈3 V vs Li^+/Li) up to 5.5 V vs Li^+/Li. The CO_2 evolution from the EC-only electrolyte (black lines, Fig. 2) starts at potentials above ≈4.6 V vs Li^+/Li and shows a strong increase above ≈4.8 V vs Li^+/Li, consistent with the report by Pritzl et al.[42] The essentially identical oxidative stability with regards to both current and CO_2 evolution is observed with FEC-only electrolyte (blue lines), indicating insignificant differences between the oxidative stability of FEC and EC up to ≈4.9 V vs Li^+/Li (even beyond this potential, the differences between current and CO_2 evolution are minor between these two electrolytes).

The essentially identical oxidative stability of EC and FEC inferred from these OEMS experiments is consistent with our findings in an earlier study,[43] but is in stark contrast with the literature, where FEC is generally considered to be oxidatively more stable at high potentials.[20,22–24,39] Thus, while the graphite//LMRNCM cycling data with upper cutoff potentials of ≈4.8 V vs Li^+/Li in the first cycle and ≈4.7 V vs Li^+/Li in all subsequent cycles (see Fig. 1) show a substantial improvement when EC is replaced by FEC, Fig. 2 clearly indicates that this cannot be due to a superior oxidative stability of FEC compared to EC. However, Jung et al.[10,11] recently suggested that electrolyte decomposition even at potentials as high as 4.8 V vs Li^+/Li is mainly caused by a *chemical* oxidation of the electrolyte solvent with lattice oxygen that is released by layered transition metal oxides at a delithiation degree of >80%, rather than by a potential-driven *electrochemical* oxidation reaction. Based on this premise, the obviously different cycle-life with EC-based versus FEC-based electrolytes (see Fig. 1) might be related to their different interaction with released lattice oxygen. Since LMRNCM cathode active materials are essentially completely delithiated in the first activation cycle,[13] most of the lattice oxygen release (as determined by OEMS analysis) will occur in the first cycle.[13,14] Therefore, to further understand the vastly different cycling performance in EC- versus FEC-based electrolytes, the following analysis focuses on the effect of this lattice oxygen release from LMRNCMs on its full-cell performance in EC- and FEC-based electrolytes.

Cycling performance of pre-activated Li- and Mn-rich NCMs.—Jung et al.[10,11] showed that lattice oxygen release from layered NCM cathodes causes strong electrolyte decomposition and is the dominating source of electrolyte decomposition up to ≈4.9 V vs Li^+/Li at 25 °C. Wandt et al.[28] and Freiberg et al.[29] proved that singlet oxygen is released from stoichiometric and from Li- and Mn-rich NCMs, and that it rapidly reacts with the electrolyte. Furthermore, as already mentioned above, the majority of the lattice oxygen release in the case of Li- and Mn-rich NCMs already occurs during the first activation cycle.[13,14,44,45] The onset potential for the first cycle oxygen release of Li- and Mn-rich NCMs was measured in previous publications from our group in EC- as well as in FEC-based electrolytes. In particular, Strehle et al.[14] conducted OEMS measurements for the first-cycle activation in an EC-based electrolyte (EC:EMC = 3:7 wt% 1M$LiPF_6$), while Teufl et al.[13] used an FEC-based electrolyte (FEC:DEC = 2:8 wt% 1M$LiPF_6$), both using comparable Li- and Mn-rich NCM materials. In both studies, the onset potential for oxygen release occurred at around 4.6 V vs Li^+/Li. This means that most of the initial electrolyte decomposition reactions triggered by lattice oxygen release from LMRNCMs are expected to be produced during the first activation cycle, producing decomposition products in the electrolyte. We here define lattice oxygen release as the loss of lattice oxygen from the near-surface region of NCMs or overlithiated NCMs at high degrees of delithiation, either in form of oxidized electrolyte species[31,32] or in form of highly reactive singlet oxygen.[28] To investigate the influence of lattice oxygen release on the full-cell capacity retention, we conducted a first-cycle pre-activation of the electrodes using graphite//LMRNCM pouch-cells, then washed the anode and cathode electrodes, and finally punched small electrodes that were reassembled in coin cells (see detailed description in the experimental section). The first-cycle pre-activation in the pouch-cells was carried out according to the same procedure that was used for the coin-cells made with pristine electrodes. The only difference in the procedure was that the pouch-cells were degassed twice during this first cycle: (i) first at 4.0 V during the first charge to remove the gases that were evolved during the SEI formation on the graphite anode; (ii) second at 4.0 V during the first discharge in order to remove the gases that were evolved during the LMRNCM activation, specifically aimed at removing the released molecular O_2 before discharging the cell to 2.0 V (corresponding to a cathode voltage of <2 V vs Li^+/Li), as it was shown that O_2 can be reduced to Li_2O_2 on the CAM surface when cycled below 3.0 V vs Li^+/Li.[13,46] In summary, this pre-activation and cell reassembly procedure allows to remove the decomposition products and the molecular oxygen produced by the high lattice oxygen release during the first activation cycle of LMRNCMs, so that the effect of lattice oxygen release on the longer-term cycling stability with different electrolytes can be examined.

The results for the pristine and the pre-activated electrodes in FEC:DEC (2:8 g:g) with 1 M $LiPF_6$ are shown in Fig. 3. It can be seen that the capacity retention of pre-activated electrodes (green symbols/lines) is superior to that of pristine electrodes (blue symbols/lines): after 90 cycles at 1 C, cells with the pre-activated electrodes have a remaining capacity of 187 ± 3 mAh g^{-1} at 1 C (i.e., at cycle #113), corresponding to 85% capacity retention at 1 C (i.e., between cycle #18 and cycle #113), while the cells with the pristine electrodes have a remaining capacity of 165 ± 3 mAh g^{-1} at 1 C, corresponding to 77% capacity retention at 1 C. Furthermore, as indicated by the essentially constant discharge capacity difference between the discharge at 0.1 C and at 1 C (see above discussion), both types of cells show no "rollover" fading, suggesting the absence of a dramatic impedance build-up. The substantial reduction of the capacity fading by the pre-activation of the electrodes in the FEC-based electrolyte strongly suggests that a substantial part of the capacity fading observed with graphite//LMRNCM cells is related to

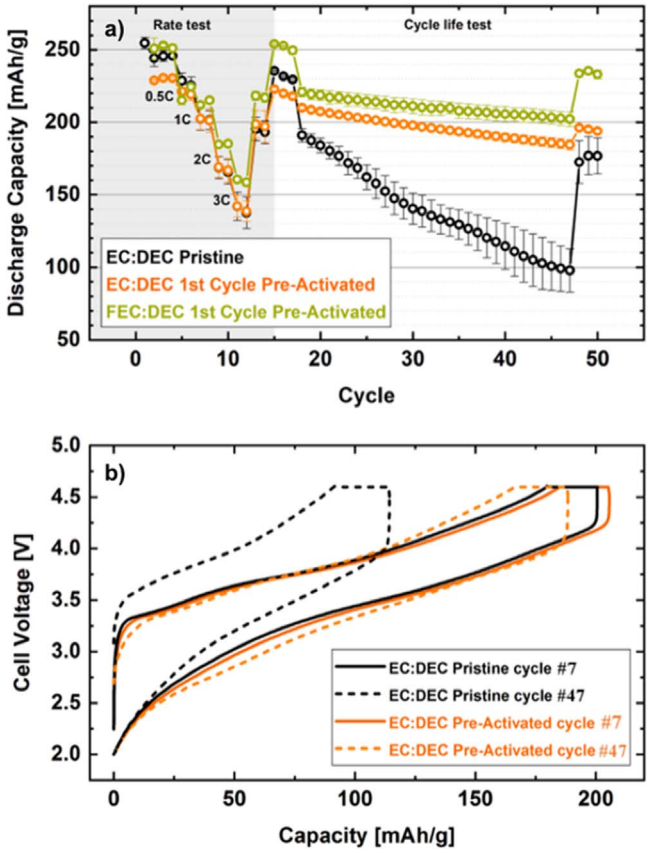

Figure 4. (a) Charge/discharge cycling of graphite//LMRNCM coin-cells (≈2.4 mAh cm^{-2}//≈1.6 mAh cm^{-2}) at 25 °C, using the same cycling procedure as in Figs. 1 and 3. Black lines/symbols: cells with pristine electrodes cycled in EC-based electrolyte (EC:DEC (2:8 g:g) with 1 M $LiPF_6$), as shown in Fig. 1; orange lines/symbols: cells with electrodes pre-activated in EC-based electrolyte and then cycled in EC-based electrolyte; green lines/symbols: cells with electrodes pre-activated and cycled in FEC-based electrolyte (FEC:DEC (2:8 g:g) with 1 M $LiPF_6$), as shown in Fig. 3. The coin-cells were assembled with 14 μl of electrolyte and with a Celgard 2500 separator; the error bars represent the minimum/maximum between three independent repeat experiments. b) Cell voltage vs capacity curves for the first cycle at 1 C discharge (cycle #7, solid lines) and for the last cycle at 1 C discharge (cycle #47, dashed lines) for a cell with pristine electrodes cycled in EC-based electrolyte (black lines) and for a cell with electrodes pre-activated and cycled in EC-based electrolyte (the charge was done at 0.7 C in both cases).

the release of lattice oxygen in the first activation cycle in combination with its effect on the *chemical* degradation of the electrolyte.

Considering that the pre-activation procedure of the electrodes seems to significantly counteract the effect of lattice oxygen release even with the FEC-based electrolyte, we will now examine whether this will also have a positive effect on the capacity fading of graphite//LMRNCM cells with an EC-based electrolyte (EC:DEC (2:8 g:g) with 1 M $LiPF_6$). Figure 4a compares the performance of the cells with pristine electrodes in the EC-based electrolyte (black symbols/lines; data from Fig. 1) with those of electrodes pre-activated in EC-based electrolyte and then cycled in EC-based electrolyte (orange symbols/lines); as reference, the performance of the cells with electrodes pre-activated and cycled in FEC-based electrolyte are also added (green symbols/lines; data from Fig. 3). In stark contrast to the rapid capacity fading of the cells with pristine electrodes and EC-based electrolyte, Fig. 4a shows that the electrodes pre-activated in EC-based electrolyte exhibit a substantially reduced capacity fading even when subsequently cycled in the EC-based electrolyte, and that they do not show any indications for an impedance build-up (suggested by the essentially constant discharge capacity difference between 0.1 C and 1 C near cycle #20 and near cycle #50). This dramatic performance improvement in EC-based electrolyte can be rationalized by the fact that in the case of pre-activated electrodes the major part of the lattice oxygen release occurs during the first activation cycle and that the associated electrolyte degradation products and the molecular O_2 were removed before the coin-cell assembly. Based on these results, we suggest that the reaction of EC with the lattice oxygen released from Li- and Mn-rich NCMs during the first activation cycle leads to a substantial impedance build-up that manifests itself in a "rollover" fading behavior. By analogy, one would expect the same phenomenon to occur when cycling stoichiometric NCMs to upper cutoff potentials that are high enough to lead to lattice oxygen release, i.e., to potentials where the NCM active material can be delithiated to ≈80% or beyond;[10,28] this would explain the "rollover" fading mechanism when cycling NCMs in EC-based electrolytes to high potentials;[10,38] this will be discussed in more detail in the next section.

To prove the hypothesis that cycling of cells with pristine electrodes in EC-based electrolyte leads to an impedance build-up and that this does not occur for cells with electrodes pre-activated and cycled in EC-based electrolyte, the cell voltage vs capacity curves for the first 1 C discharge cycle and the last 1 C discharge cycle (cycle #7 and cycle #47) for the cells with pristine and with the pre-activated electrodes are shown in Fig. 4b (for both cycles, the charge rate was 0.7 C). In cycle #7 (solid lines), the voltage profiles for the pristine and the pre-activated materials are essentially identical and have very similar capacity. The picture changes for cycle #47 (dashed lines): while the cell with the pre-activated electrodes only shows very slightly increased overpotentials (reflected by a negligible increase in the width of the curve), the cell with the pristine electrodes not only shows a much lower capacity, but also much larger overpotentials. Thus, the cell voltage vs capacity curves clearly show that the combination of lattice oxygen release during the first activation cycle and the use of an EC-based electrolyte leads to a high impedance build-up that is reflected in a "rollover" fading mechanism.

There is an ongoing discussion in the literature about the exact decomposition mechanism of EC during the lattice oxygen release at high degrees of delithiation. Wandt et al.[28] clearly showed that at least a part of the released lattice oxygen from NCMs and LMRNCMs is formed as singlet oxygen, and that its appearance coincides with the onset of O_2 and CO_2 evolution. Based on this observation, Freiberg et al.[29] conducted an experiment in which EC was exposed to singlet oxygen, by which they could show that singlet oxygen reacts with EC, forming vinylene carbonate (VC) and hydrogen peroxide (H_2O_2). They also showed that H_2O_2 gets electrochemically oxidized at potentials >4.5 V vs Li^+/Li to water and protons, which are expected to lead to further electrolyte degradation and transition metal dissolution. Furthermore, Pritzl et al. showed that VC gets electrochemically oxidized at potentials exceeding ≈4.3 V vs Li^+/Li, yielding next to CO_2 also poly-VC that largely increases the cathode impedance and leads to a "rollover" failure in cycle-life tests.[42] Based on this previous work, we suggest that the cell impedance increase that leads to the "rollover" failure and which is shown in Fig. 4b is likely due to an increase of the cathode impedance, caused due to the oxidation of VC at these high potentials.[42] An alternative mechanism for the degradation of EC at high degrees of delithiation was proposed by Yu et al.,[31] who suggested a dehydrogenation reaction of EC triggered by activated oxygen on the surface of layered transition metal oxide based CAMs, leading to a ring-opening and oligomerization of EC. Which of these two proposed EC decomposition mechanisms is the predominant one is still being debated, but both mechanisms could explain the impedance build-up and the associated "rollover" fading upon lattice oxygen release that can be deduced from Fig. 4. As mentioned above, the formation of VC by the reaction of EC with singlet oxygen would lead to poly-VC deposits on the CAM surface

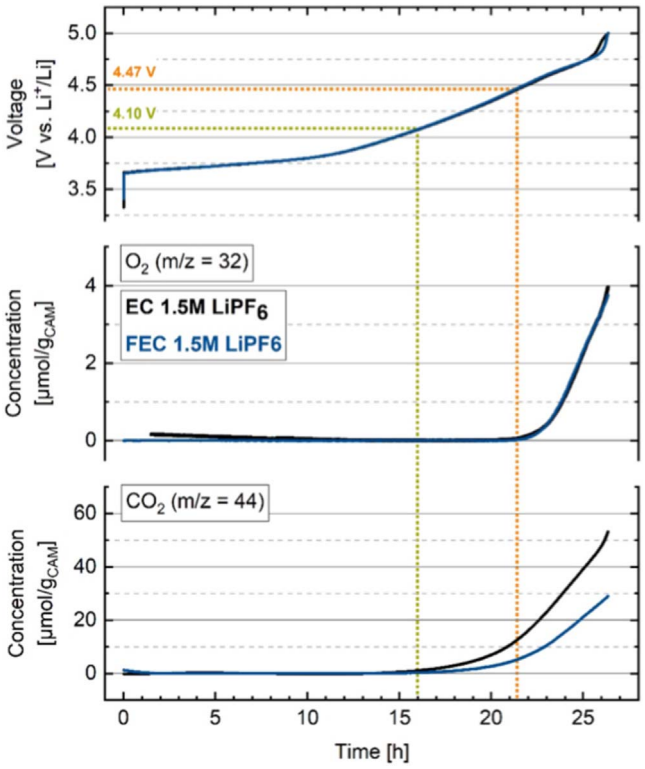

Figure 5. OEMS measurements for the first galvanostatic charge in a one-compartment OEMS cell with an NCM-622 working electrode and a lithium counter electrode using an EC-only electrolyte (EC + 1.5 M $LiPF_6$; black lines) or an FEC-only electrolyte (FEC + 1.5 M $LiPF_6$; blue lines) at 25 °C. Upper panel: cell voltage vs time (note: 1 h corresponds to a charge of 10.7 mAh g^{-1}); middle/lower panel: evolution of the concentration of concomitantly evolved O_2/CO_2 given in μmol/g_{AM}. Cells were charged galvanostatically at a C/15 rate (referenced to a nominal capacity of 160 mAh g^{-1}) from OCV (≈3 V) to 5.0 V. The dotted green line indicates the CO_2 onset potential at ≈4.10 V vs Li^+/Li and the dotted orange line indicates the onset potential for O_2 evolution at ≈4.47 V vs Li^+/Li.

that cause an impedance build-up and a rapid cell failure.[42] On the other hand, the EC dehydrogenation proposed by Yu et al.[31] could lead to oligomerization of EC that in turn might also form resistive polymer layers on the active materials and a concomitant impedance build-up.[31] Again, while the exact mechanism is still under discussion, the data shown in Figs. 1 and 4 clearly indicate that the reaction product(s) of EC with (released) lattice oxygen lead to a rapid impedance build-up, a phenomenon that is not observed with FEC-based, EC-free electrolyte.

Relevance of lattice oxygen release for stoichiometric NCMs.— So far, we only focused on the performance differences of Li- and Mn-rich NCMs when cycled in full-cells with either EC- or FEC-based electrolytes, demonstrating that the reaction products of EC with released lattice oxygen lead to a drastic impedance build-up. In the following, we will now examine the impact of lattice oxygen release onto the cycling performance of an NCM-622 active material in full-cells with EC- vs FEC-based electrolyte, selecting the upper cutoff cell voltage such that it is either below or above the potential for lattice oxygen release. Again we define lattice oxygen release as the loss of lattice oxygen from the near-surface region of NCMs or overlithiated NCMs at high degrees of delithtiation, either in form of oxidized electrolyte species[31,32] or in form of highly reactive singlet oxygen.[28] To determine this onset potential, we will first conduct OEMS experiments with an NCM-622 working electrode and a lithium metal counter electrode in a one-compartment OEMS cell, using the EC-only and FEC-only model electrolytes containing 1.5 M $LiPF_6$ that were already used for the experiments shown in Fig. 2.

The upper panel of Fig. 5 shows the galvanostatic charging profile of the NCM-622 working electrode in a one-compartment OEMS cell from OCV (≈3 V) up to 5.0 V, measured against a lithium counter electrode, in both EC-only electrolyte (black line) and FEC-only electrolyte (blue line). The data were acquired at a rate of C/15 (referenced to 160 mAh g^{-1}) and the voltage profiles are essentially identical with both electrolytes; furthermore, the same total capacity of ≈ 265 mAh g^{-1} is reached upon charge to 5.0 V vs Li^+/Li, which is very close to the theoretical capacity of ≈277 mAh g^{-1} for a complete delithiation. The middle/lower panels depict the concentration of the evolved O_2 (m/z = 32, middle panel) and CO_2 (m/z = 44, lower panel) given in μmol/g_{AM}. In line with the identical voltage profiles, also the oxygen evolution profiles are identical for the two different electrolytes, whereby the onset potential for oxygen evolution is at ≈4.47 V vs Li^+/Li (see orange dotted lines in Fig. 5). The accumulated delithiation charge at the onset potential for oxygen evolution (i.e., after ≈21.2 h of charge) corresponds to ≈226 mAh g^{-1} which, if referenced to the theoretical delithiation capacity of ≈277 mAh/g for NCM-622, equates to a theoretical state-of-charge of ≈82%. This is perfectly consistent with previous measurements from our group, where we had found that O_2 evolution from NCMs and LMRNCMs always occurs at ≈80% delithiation (if referenced to the theoretical delithiation capacity),[10,11,13,14,28] even at elevated temperatures.[34]

The onset of O_2 evolution is followed by a clearly increasing rate of CO_2 evolution (Fig. 5, bottom panel), which is in good accordance with the results reported by Jung et al.[10,34] However, a first onset for CO_2 evolution can be observed in both electrolytes starting at ≈4.10 V vs Li^+/Li (see green dotted lines in Fig. 5). Based on the hypothesis proposed by Jung et al.,[34] this initial CO_2 evolution wave in OEMS experiments with NCM-622 (and, by extension, with other NCM compositions) stems from the reaction of electrolyte impurities (water, alcohols, and other protic species) and perhaps hydroxide-based CAM surface impurities, while the CO_2 evolution at higher potentials can be rationalized by the reaction of lattice oxygen with the electrolyte, similar as reported for Li- and Mn-rich NCMs.[13,14] While the O_2 evolution profile is identical for both electrolytes (Fig. 5, middle panel), the CO_2 evolution profiles are different, resulting in a ≈2-fold higher total amount of CO_2 produced by the end of the galvanostatic charge in the EC-based electrolyte (≈55 μmol g^{-1}) compared to the FEC-based electrolyte (≈30 μmol g^{-1}). These different amounts of evolved CO_2 already indicate different chemical degradation mechanisms for EC and for FEC, which is the likely origin for the observation that cycling LMRNCMs in EC-based electrolytes leads to an obvious impedance build-up upon cycling (see black symbols/lines in Fig. 1 and black lines in Fig. 4), while this is not observed for FEC-based electrolytes (see blue symbols/lines in Fig. 1).

In summary, our data suggest that the products of the reaction of EC with released lattice oxygen lead to the observed high impedance build-up upon cycling and that they are much more detrimental for the full-cell performance than the products produced by the reaction of FEC with released lattice oxygen. To further prove this hypothesis, graphite//NCM-622 full-cells were assembled with EC-based electrolyte (EC:DEC (2:8 g:g) with 1 M $LiPF_6$) or with FEC-based electrolyte (FEC:DEC (2:8 g:g) with 1 M $LiPF_6$) and cycled below and above the onset potential for oxygen evolution. If our hypothesis were to be correct, the use of an EC-based electrolyte above the onset potential for oxygen evolution should lead to a "rollover" fading behavior. The oxygen onset potential of ≈4.47 V vs Li^+/Li for the here examined NCM-622 CAM (Fig. 5) corresponds to an upper cutoff cell voltage in a graphite//NCM-622 full-cell of ≈ 4.37 V and will serve as guideline for the cycling experiments.

In order to investigate the effect of lattice oxygen release from stoichiometric NCMs on their cycling performance with EC- or FEC-based electrolytes, we will now examine the cycling performance of graphite//NCM-622 full-cells with either EC-based

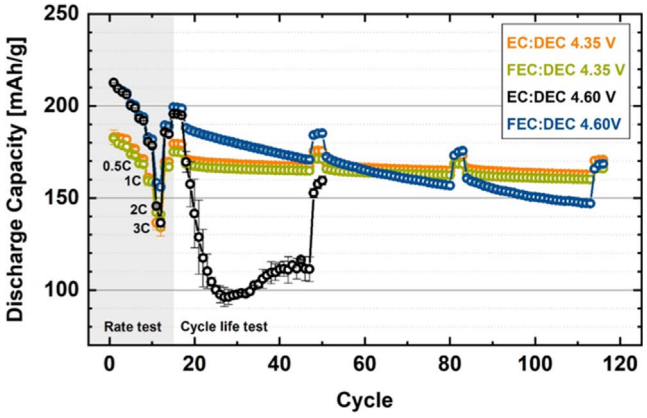

Figure 6. Charge/discharge cycling to different upper cutoff cell voltages of graphite//NCM-622 coin-cells at 25 °C using a Celgard 2500 separator and 21 μl of either an EC-based electrolyte (EC:DEC (2;8 g g^{-1}) with 1 M $LiPF_6$) or an FEC-based electrolyte (FEC:DEC (2:8 g:g with 1 M $LiPF_6$). The upper cutoff cell voltages were either 4.35 V (i.e., below the onset potential for O_2 evolution) or 4.60 V (i.e., above the onset potential for O_2 evolution), while the lower cutoff cell voltage was kept at 3.0 V. All cells underwent the same cycling procedure as that used in Fig. 1: activation at C/15 (C-rates here are referenced to a nominal capacity of 160 mAh g^{-1}), a rate test (discharge rates are indicated in the figure) that is marked by the gray shaded area, then a longer-term cycling sequence starting with 3 cycles at 0.1 C (CC) charge and 0.1 C (CC) discharge followed by 30 cycles at 0.7 C (CCCV) charge and 1 C discharge (CC) (this sequence was repeated several times, ending with 3 cycles at 0.1 C (CC) charge and 0.1 C (CC) discharge). The error bars represent the minimum/maximum between three independent repeat experiments. The areal capacity of the graphite electrodes was 3.0 mAh cm^{-2} and that of the NCM-622 electrodes was 1.6 mAh cm^{-2} (referenced to a nominal capacity of 160 mAh g^{-1}).

electrolytes (EC:DEC (2:8 g:g) with 1 M $LiPF_6$) or FEC-based electrolytes (FEC:DEC (2:8 g:g) with 1 M $LiPF_6$). One set of the cells were cycled to an upper cutoff cell voltage of 4.35 V (corresponding to ≈4.45 V vs Li^+/Li), which is slightly below the onset potential for oxygen evolution of ≈4.47 V vs Li^+/Li (Fig. 5), while another set of cells were cycled to an upper cell voltage of 4.60 V (corresponding to ≈4.7 V vs Li^+/Li), which is above the onset potential for oxygen evolution, but where the purely *electrochemical* oxidation of EC and FEC is still rather small (Fig. 2). Except for the different upper cutoff cell voltages, these graphite//NCM-622 cells were cycled with the same protocol that was used for the Li- and Mn-rich NCMs shown before (see, e.g., Fig. 1). Figure 6 depicts the results of the cycling experiments, it can be seen that for the cells cycled to an upper cutoff cell voltage of 4.35 V (orange and green symbols/lines), both the EC- and the FEC-based electrolytes show good and essentially identical cycling performance under this condition where no lattice oxygen release occurs.

In stark contrast, when the cells are cycled to an upper cutoff cell voltage that is beyond the onset potential for oxygen evolution, a strong deviation is observed between the cells using EC-based electrolyte (black symbols/lines in Fig. 6) and those using FEC-based electrolyte (blue symbols/lines Fig. 6). The cells with the FEC-based electrolyte show a gradual and continuous capacity decay, with a remaining capacity at 1 C after 47 cycles of ≈171 ± 1 mAh g^{-1}, while the cells with the EC-based electrolyte that initially have the same capacity as the cells with the FEC-based electrolyte very quickly lose capacity and after 47 cycles the remaining capacity at a 1 C discharge is only ≈111 ± 7 mAh g^{-1}. As was observed for graphite//LMRNCM cells with EC-based electrolyte (Fig. 1), the discharge capacity difference between 0.1 C and 1 C discharge increases with cycling for the cells with EC-based electrolyte that are cycled above the onset potential for oxygen evolution (black symbols/line in Fig. 6), reaching a difference of ≈50 mAh g^{-1} after the first 1 C cycling sequence (near cycle #50). This clearly points towards a substantial impedance build-up over only ≈50 cycles. This discharge capacity difference between 0.1 C and 1 C discharge is substantially smaller for the FEC-based electrolyte after ≈50 cycles (≈15 mAh g^{-1}), but also gradually increases over ≈120 cycles to ≈20 mAh g^{-1} (blue symbols/line in Fig. 6). The fact that the capacity fading of the cells with the FEC-based electrolyte is clearly much worse when the upper cutoff cell voltage is 4.60 V (blue symbols/line in Fig. 6) compared to an upper cutoff cell voltage of 4.35 V (green symbols/line in Fig. 6) can be explained by a combination of the degradation of the cathode active material due to the lattice oxygen release and the *chemical* reaction of FEC the released lattice oxygen; a purely *electrochemical* oxidation of FEC would also be possible, but based on the OEMS based stability data in Fig. 2 this is likely a more minor effect. Although the cells with the FEC-based electrolyte do not suffer from a large impedance build-up even when cycled to upper cutoff cell potentials of 4.6 V, lattice oxygen release might still lead to electrolyte decomposition products that could lead to the decomposition of the conductive salt,[27,47] to transition metal migration, [48–50] and/or clogging of the separator pores. While these effects need further study, it can, however, be concluded that the detrimental effects of lattice oxygen release on cycle-life are substantially more pronounced with EC-based electrolytes compared to FEC-based and EC-free electrolytes.

Conclusions

In this study we examined the high-voltage cycling performance of stoichiometric NCM and of Li- and Mn-rich NCM (LMRNCM) cathode active materials (CAMs) in graphite//CAM full-cells with either EC-based or FEC-based and EC-free electrolytes. In particular, we could show that LMRNCMs that have to be cycled to upper cutoff potentials of ≈4.7 V vs Li^+/Li in order to reach their full capacity have a very poor cycle-life in EC-based electrolytes, largely due to a rapid impedance build-up that is accompanied by a so-called "rollover" failure. On the other hand, the cycle-life of graphite//LMRNCM coin-cells was substantially improved with an FEC-based and EC-free electrolyte, for which no impedance build-up was observed.

While the generally superior high-voltage performance of FEC-based and EC-free electrolytes is commonly believed to be due to the higher stability of FEC towards *electrochemical* oxidation at high potentials, we could show by on-line electrochemical mass spectrometry (OEMS) that the anodic stability of EC is essentially identical with that of FEC, so that there must be a different reason for the superior cycle-life of graphite//LMRNCM full-cells with FEC-based and EC-free electrolyte.

One possible alternative explanation might be a different reactivity of EC and FEC with the oxygen evolved from layered transition metal oxides at high degrees of delithiation. As this oxygen release with LMRNCMs occurs mostly in the first activation cycle, we compared the cycle-life of graphite//LMRNCM cells built with either pristine electrodes or with electrodes harvested after the first activation cycle. In the latter case, the cycle-life with EC-based electrolyte closely approached that of the FEC-based and EC-free electrolyte, proving the hypothesis that the fundamental difference between EC and FEC with regards to high-voltage performance with layered transition metal oxides is due to their different reactivity with released lattice oxygen.

This was confirmed by cycling experiments with graphite//NCM-622 coin-cells, where it could be shown that the performance with an EC-based electrolyte is identical with that of an FEC-based and EC-free electrolyte, if the upper cutoff potential is below the onset potential for O_2 evolution of the NCM-622 CAM (shown by OEMS measurements to be at ≈4.47 V vs Li^+/Li). On the other hand, for an upper cutoff potential above the onset potential for O_2 evolution, the performance of the graphite//NCM-622 cells was very poor with the EC-based electrolyte, showing the same rapid impedance build-up and "rollover" failure as was observed with LMRNCMs.

Acknowledgments

This work was supported by BASF SE within its BASF SE Battery Research Network.

ORCID

Tobias Teufl https://orcid.org/0000-0001-5889-5204

References

1. D. Larcher and J. M. Tarascon, *Nat. Chem.*, **7**, 19 (2015).
2. J. B. Goodenough and K. S. Park, *J. Am. Chem. Soc.*, **135**, 1167 (2013).
3. M. M. Thackeray, C. Wolverton, and E. D. Isaacs, *Energy & Environ. Sc.*, **5**, 7854 (2012).
4. D. Andre, S.-J. Kim, P. Lamp, S. F. Lux, F. Maglia, O. Paschos, and B. Stiaszny, *J. Mat. Chem. A*, **3**, 6709 (2015).
5. K. Mizushima, P. Jones, P. Wiseman, and J. B. Goodenough, *Mater. Res. Bull.*, **15**, 783 (1980).
6. M. M. Thackeray, S.-H. Kang, C. S. Johnson, J. T. Vaughey, R. Benedek, and S. A. Hackney, *J. Mater. Chem.*, **17**, 3112 (2007).
7. K. G. Gallagher, S. Goebel, T. Greszler, M. Mathias, W. Oelerich, D. Eroglu, and V. Srinivasan, *Energy Environ. Sci.*, **7**, 1555 (2014).
8. S. Hy, H. Liu, M. Zhang, D. Qian, B.-J. Hwang, and Y. S. Meng, *Energy Environ. Sci.*, **9**, 1931 (2016).
9. J. R. Croy, M. Balasubramanian, K. G. Gallagher, and A. K. Burrell, *Acc. Chem. Res.*, **48**, 2813 (2015).
10. R. Jung, M. Metzger, F. Maglia, C. Stinner, and H. A. Gasteiger, *J. Electrochem. Soc.*, **164**, A1361 (2017).
11. R. Jung, M. Metzger, F. Maglia, C. Stinner, and H. A. Gasteiger, *J. Phys. Chem. Lett.*, **8**, 4820 (2017).
12. D. Streich, C. Erk, A. Guéguen, P. Müller, F.-F. Chesneau, and E. J. Berg, *J. Phys. Chem. C*, **121**, 13481 (2017).
13. T. Teufl, B. Strehle, P. Müller, H. A. Gasteiger, and M. A. Mendez, *J. Electrochem. Soc.*, **165**, A2718 (2018).
14. B. Strehle, K. Kleiner, R. Jung, F. Chesneau, M. Mendez, H. A. Gasteiger, and M. Piana, *J. Electrochem. Soc.*, **164**, A400 (2017).
15. T. Teufl, D. Pritzl, S. Solchenbach, H. A. Gasteiger, and M. A. Mendez, *J. Electrochem. Soc.*, **166**, A1275 (2019).
16. J. Xia, M. Nie, J. C. Burns, A. Xiao, W. M. Lamanna, and J. R. Dahn, *J. Power Sources*, **307**, 340 (2016).
17. J. Xia, K. J. Nelson, Z. Lu, and J. R. Dahn, *J. Power Sources*, **329**, 387 (2016).
18. J. Xia, R. Petibon, D. Xiong, L. Ma, and J. R. Dahn, *J. Power Sources*, **328**, 124 (2016).
19. R. Petibon, J. Xia, L. Ma, M. K. G. Bauer, K. J. Nelson, and J. R. Dahn, *J. Electrochem. Soc.*, **163**, A2571 (2016).
20. L. Ma, S. L. Glazier, R. Petibon, J. Xia, J. M. Peters, Q. Liu, J. Allen, R. N. C. Doig, and J. R. Dahn, *J. Electrochem. Soc.*, **164**, A5008 (2016).
21. A. J. Gmitter, I. Plitz, and G. G. Amatucci, *J. Electrochem. Soc.*, **159**, A370 (2012).
22. K. Xu, *Chem. Rev.*, **114**, 11503 (2014).
23. L. Hu, Z. Zhang, and K. Amine, *Electrochem. Commun.*, **35**, 76 (2013).
24. L. Hu, Z. Xue, K. Amine, and Z. Zhang, *J. Electrochem. Soc.*, **161**, A1777 (2014).
25. E. Markevich, G. Salitra, K. Fridman, R. Sharabi, G. Gershinsky, A. Garsuch, G. Semrau, M. A. Schmidt, and D. Aurbach, *Langmuir*, **30**, 7414 (2014).
26. B. Aktekin, R. Younesi, W. Zipprich, C. Tengstedt, D. Brandell, and K. Edström, *J. Electrochem. Soc.*, **164**, A942 (2017).
27. T. Teufl, D. Pritzl, L. Hartmann, S. Solchenbach, M. Mendez, and H. A. Gasteiger, *In Press*.
28. J. Wandt, A. T. S. Freiberg, A. Ogrodnik, and H. A. Gasteiger, *Mater. Today*, **21**, 218 (2018).
29. A. T. S. Freiberg, M. K. Roos, J. Wandt, R. de Vivie-Riedle, and H. A. Gasteiger, *J. Phys. Chem. A*, **122**, 8828 (2018).
30. T. M. Østergaard, L. Giordano, I. E. Castelli, F. Maglia, B. K. Antonopoulos, Y. Shao-Horn, and J. Rossmeisl, *J. Phys. Chem. C*, **122**, 10442 (2018).
31. Y. Yu, P. Karayaylali, Y. Katayama, L. Giordano, M. Gauthier, F. Maglia, R. Jung, I. Lund, and Y. Shao-Horn, *J. Phys. Chem. C*, **122**, 27368 (2018).
32. L. Giordano, P. Karayaylali, Y. Yu, Y. Katayama, F. Maglia, S. Lux, and Y. Shao-Horn, *J. Phys. Chem. Lett.*, **8**, 3881 (2017).
33. F. T. Wagner, B. Lakshmanan, and M. F. Mathias, *J. Phys. Chem. Lett.*, **1**, 2204 (2010).
34. R. Jung, P. Strobl, F. Maglia, C. Stinner, and H. A. Gasteiger, *J. Electrochem. Soc.*, **165**, A2869 (2018).
35. N. Tsiouvaras, S. Meini, I. Buchberger, and H. A. Gasteiger, *J. Electrochem. Soc.*, **160**, A471 (2013).
36. M. Metzger, B. Strehle, S. Solchenbach, and H. A. Gasteiger, *J. Electrochem. Soc.*, **163**, A798 (2016).
37. F. J. Günter, C. Burgstaller, F. Konwitschny, and G. Reinhart, *J. Electrochem. Soc.*, **166**, A1709 (2019).
38. J. C. Burns, A. Kassam, N. N. Sinha, L. E. Downie, L. Solnickova, B. M. Way, and J. R. Dahn, *J. Electrochem. Soc.*, **160**, A1451 (2013).
39. Z. Zhang, L. Hu, H. Wu, W. Weng, M. Koh, P. C. Redfern, L. A. Curtiss, and K. Amine, *Energy Environ. Sci.*, **6**, 1806 (2013).
40. M. Metzger, C. Marino, J. Sicklinger, D. Haering, and H. A. Gasteiger, *J. Electrochem. Soc.*, **162**, A1123 (2015).
41. M. Metzger, P. Walke, S. Solchenbach, G. Salitra, D. Aurbach, and H. A. Gasteiger, *In Press*.
42. D. Pritzl, S. Solchenbach, M. Wetjen, and H. A. Gasteiger, *J. Electrochem. Soc.*, **164**, A2625 (2017).
43. S. Solchenbach, M. Metzger, and H. A. Gasteiger, *Meeting Abstracts*, **MA2015-02**, 362 (2015).
44. A. R. Armstrong, M. Holzapfel, P. Novák, C. S. Johnson, S.-H. Kang, M. M. Thackeray, and P. G. Bruce, *J. Am. Chem. Soc.*, **128**, 8694 (2006).
45. T. Zünd, B. Strehle, D. Hochfilzer, and H. A. Gasteiger, *In Press*.
46. N. Yabuuchi, K. Yoshii, S. T. Myung, I. Nakai, and S. Komaba, *J. Am. Chem. Soc.*, **133**, 4404 (2011).
47. A. Guéguen, D. Streich, M. He, M. Mendez, F. F. Chesneau, P. Novák, and E. J. Berg, *J. Electrochem. Soc.*, **163**, A1095 (2016).
48. J. A. Gilbert, I. A. Shkrob, and D. P. Abraham, *J. Electrochem. Soc.*, **164**, A389 (2017).
49. R. Jung, F. Linsenmann, R. Thomas, J. Wandt, S. Solchenbach, F. Maglia, C. Stinner, M. Tromp, and H. A. Gasteiger, *J. Electrochem. Soc.*, **166**, A378-A (2019).
50. J. Wandt, A. Freiberg, R. Thomas, Y. Gorlin, A. Siebel, R. Jung, H. A. Gasteiger, and M. Tromp, *J. Mater. Chem. A*, **4**, 18300 (2016).